Biosensors and Bioelectronics 74 (2015) 660–665

Contents lists available at ScienceDirect

Biosensors and Bioelectronics

journal homepage: www.elsevier.com/locate/bios

In situ deposition of Prussian blue on mesoporous carbon nanosphere for sensitive electrochemical immunoassay

Guosong Lai [a,b,*], Haili Zhang [a], Aimin Yu [a,c,*], Huangxian Ju [b]

[a] Hubei Collaborative Innovation Center for Rare Metal Chemistry, Hubei Key Laboratory of Pollutant Analysis & Reuse Technology, Department of Chemistry, Hubei Normal University, Huangshi 435002, PR China

[b] State Key Laboratory of Analytical Chemistry for Life Science, Department of Chemistry, Nanjing University, Nanjing 210093, PR China

[c] Department of Chemistry and Biotechnology, Faculty of Science, Engineering and Technology, Swinburne University of Technology, Hawthorn VIC 3122, Australia

ARTICLE INFO

Article history:
Received 26 May 2015
Received in revised form
10 July 2015
Accepted 11 July 2015
Available online 14 July 2015

Keywords:
Biosensor
Electrochemical immunoassay
Signal amplification
Prussian blue
Carbon nanosphere

ABSTRACT

A Prussian blue (PB) functionalized mesoporous carbon nanosphere (MCN) composite was prepared for loading signal antibody and high-content glucose oxidase (GOD) to obtain a new nanoprobe for sensitive electrochemical immunoassay. The MCN nanocarrier with an average diameter of 180 nm was synthesized by using mesoporous silica nanosphere as a hard template in combination with a hydrothermal carbonization method. This hydrophilic carbon nanomaterial provided an ideal platform for in situ deposition of high-content PB to form the MCN-PB nanocomposite. Based on the step-wise assembly of polyelectrolyte and gold nanoparticles (Au NPs) on the negative-charged nanocomposite, signal antibody and high-content GOD were loaded on this nanocarrier to obtain the nanoprobe. After a sandwich immunoreaction at an Au NPs-modified screen-printed carbon electrode based immunosensor, the nanoprobes were quantitatively captured on the electrode surface to produce sensitive electrochemical response with a PB-mediated GOD catalytic reaction for immunoassay. The high loading of PB and GOD on the nanoprobe greatly amplified the electrochemical signal, leading to the development of a new immunoassay method with high sensitivity. Using human immunoglobulin G as a model analyte, excellent analytical performance including a wide linear range from 0.01 to 100 ng/mL and a low detection limit down to 7.8 pg/mL was obtained. Additionally, the immunosensor showed high specificity, satisfactory stability and repeatability as well as acceptable reliability. The PB-mediated GOD electrochemical system well excluded the conventional interference from the dissolved oxygen. Thus this immunoassay method provides great potentials for practical applications.

1. Introduction

The development of electrochemical chip based immunosensors for sensitive measurement of protein biomarkers has shown great application potentials for point-of-care diagnosis (Wan et al., 2013; Rusling, 2013; Lai et al., 2014a). In order to achieve the accurate measurement of low-abundant biomarkers for early disease diagnosis, various strategies, especially various nano signal amplification strategies have been developed recently. Commonly, the excellent electroconductivity and biocompatibility of nanomaterials enable their wide application in the construction of versatile nanosensing surfaces with good bioaffinity and electron transfer ability (Malhotra et al., 2010; Haque et al., 2012). More importantly, the high specific surface area of nanomaterials makes them to be served as ideal nanocarriers for loading high-content signal tags and designing various useful nanoprobes for immunoassays (Song et al., 2010; Chikkaveeraiah et al., 2012; Ji et al., 2015). Up to now a great variety of nanomaterials, especially various carbon nanomaterials such as carbon nanotubes (CNTs) (Yu et al., 2006; Lai et al., 2011) and graphene (Du et al., 2011; Wen et al., 2014), have been widely used for the nanoprobe preparation owing to their exceptional electrical, thermal, chemical and mechanical properties, which dramatically enhanced the signal responses of the sandwich immunorecognition events and thus greatly improved the analytical sensitivity of these immunoassay methods.

As a kind of useful carbon nanomaterial, carbon nanosphere has also shown successful application in this field. For example, Cui (Cui et al., 2008) and Xu (Xu et al., 2012) designed two types of nanoprobes for electrochemical immunoassay using carbon nanospheres to load high-content horseradish peroxidase (HRP) and gold nanoparticle (Au NP) tags. Significantly, in order to further

* Corresponding authors.
E-mail addresses: gslai@hbnu.edu.cn (G. Lai), aiminyu@swin.edu.au (A. Yu).

http://dx.doi.org/10.1016/j.bios.2015.07.026
0956-5663/

improve the analytical performance of immunoassay methods for achieving higher sensitivity, an increasing number of researches are focused on the development of new nanocarriers, especially mesoporous nanomaterials which possess larger specific surface area and are able to load higher content of signal tags in the latest years (Yang et al., 2010; Li et al., 2011a). Although mesoporous carbon nanosphere (MCN) might be the best candidate as the mesoporous nanocarrier, its irregular particle shape with large average size over 1 μm and the inherent hydrophobicity accompanied with the conventional preparation under rather harsh conditions greatly limit its applications in the bioassay field (Wan et al., 2008; Hu et al., 2010; Gu et al., 2011). As a cheap, mild and absolutely "green" approach newly rising in recent years, hydrothermal carbonization provides a new route for synthesis of various carbon nanomaterials with tunable structure and size character. Additionally, it can also produce abundant oxygen-containing groups such as COOH, OH, C=O on the surface of the materials (Titirici and Antonietti, 2010; Fang et al., 2010; Li et al., 2011b). These groups greatly improve the water dispersibility of carbon nanomaterials and also provide an ideal interface for further functionalization with various signal tags.

Among the electrochemical tags, Prussian blue (PB) is a well-known "artificial peroxidase" that has gained distinctive attentions in the biosensing field owing to its low cost and selective electrocatalytic reduction of H_2O_2 in the coexistence of oxygen (Karyakin et al., 2000; Li et al., 2007). Previously, we designed a glucose oxidase (GOD) functionalized CNT nanoprobe for the signal tracing of a screen-printed carbon electrode (SPCE) based immunosensor by coupling with PB-mediated enzymatic cycle, which successfully overcame the interference problem of dissolved oxygen in the conventional HRP-based electrochemical immunoassays (Lai et al., 2009). However, the large background current from the PB immobilized on the electrode surface restricted the sensitivity in some degree. Additionally, PB was chemically synthesized by mixing ferric and hexacyanoferrate ions with the different oxidation state of iron: either $Fe^{3+}+[Fe^{II}(CN)_6]^{4-}$ or $Fe^{2+}+[Fe^{III}(CN)_6]^{3-}$ (Karyakin, 2001; Ricci and Palleschi, 2005). However, the reaction between the two agents was too fast to be able to control the product, which resulted in its poor repeatability for the sensing applications. Recent research has shown that the inherent weak reduction property of carbon nanomaterials including CNTs and graphene can slowly reduce ferric ions resulting in the formation of PB nanocrystals in the presence of $[Fe^{III}(CN)_6]^{3-}$ (Zhai et al., 2009; Jin et al., 2010). This phenomenon provides a promising way for the controllable preparation of PB-carbon nanocomposites.

In view of this, in this work a kind of MCN with an average diameter of 180 nm was firstly synthesized using mesoporous silica nanosphere as template in combination with the hydrothermal carbonization method. PB was then in situ deposited on this nanocarrier to obtain a MCN-PB nanocomposite. After the step-wise assembly of polyelectrolyte and Au NPs for further loading signal antibody and high-content GOD on this nanocomposite, a new nanoprobe was successfully prepared for the electrochemical immunoassay (Scheme 1). Upon performing the sandwich immunoreaction at an Au NPs-modified SPCE-based immunosensor, the nanoprobes were quantitatively captured on the electrode surface to form the immunocomplex and then produced sensitive electrochemical signal for immunoassay through the PB-mediated GOD catalytic reaction, which excluded the interference from dissolved oxygen completely. Due to the high loading of PB and GOD on the nanoprobe for signal amplification as well as the enzymatically catalytic reaction, a sensitive immunoassay method was successfully developed for the accurate measurement of the protein analyte of human immunoglobulin G (HIgG).

2. Materials and methods

2.1. Materials and reagents

Human immunoglobulin G (HIgG), mouse immunoglobulin G (MIgG) and polyclonal rabbit anti-human immunoglobulin G (anti-HIgG) were purchased from Wuhan Boster Biological Technology Ltd. Carcinoembryonic antigen (CEA) was purchased from Xiamen Boson Biotechnology Ltd. Glucose oxidase (GOD, from Aspergillus niger), tetraethoxysilane (TEOS), Pluronic® F-127, hexadecyltrimethylammonium bromide (CTAB), furfural, poly(diallyldimethylammonium chloride) (PDDA, 20%, w/w in water), bovine serum albumin (BSA) and human serum albumin (HSA) were obtained from Sigma-Aldrich Chemical Co. Chloroauric acid ($HAuCl_4 \cdot 4H_2O$) and trisodium citrate were obtained from Shanghai Reagent Company. The bovine serum was obtained from Beijing Solarbio Science & Technology Ltd. All other reagents were of analytical reagent grade and used without further purification. Doubly distilled water was used throughout the experiments.

Phosphate-buffered saline (PBS) solutions at various pH values were prepared by mixing the stock solutions of 50 mM NaH_2PO_4 and Na_2HPO_4. A 50 mM pH 7.0 PBS containing 0.05% (*w*/*v*) Tween-20 (PBST) was used as washing buffer, and a 50 mM pH 7.0 PBS containing 2% (*w*/*v*) BSA was used as blocking solution. In addition, a 50 mM pH 6.9 PBS containing 10 mM glucose was used as the substrate solution.

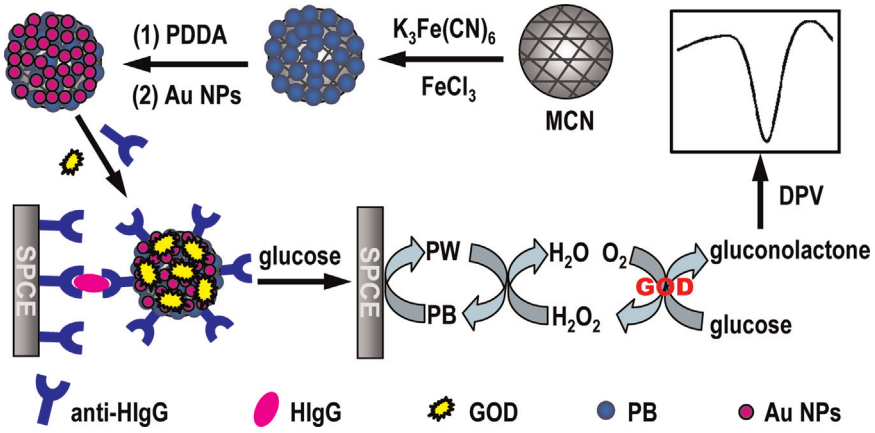

Scheme 1. Schematic representation of the preparation of MCN-PB based nanoprobe and the electrochemical detection strategy of the immunoassay method.

2.2. Apparatus

All electrochemical experiments were performed on a CHI 430A electrochemical workstation (USA). The UV–vis measurements were carried out on a UV-3100 spectrophotometer (Hitachi, Japan). The FTIR spectra were recorded on a Thermo Scientific Nicolet iD5 spectrometer. The scanning electron microscopic (SEM) images and energy-dispersive X-ray (EDX) spectrum were examined using a FEI Quanta 400F scanning electron microscope. The transmission electron microscopic (TEM) images were obtained with a JEOL 1010 transmission electron microscope. The powder X-ray diffraction (XRD) pattern was measured on a Rigaku Ultima IV X-Ray diffractometer. The zeta potential analysis was performed with a Brookhaven 90Plus particle size analyzer.

2.3. Preparation of MCN-PB nanocomposite

Firstly, the mesoporous silica nanosphere was synthesized with a modified Stöber method (Gu et al., 2011; Kim et al., 2008). Briefly, 0.5 g of CTAB and 2.05 g Pluronic® F-127 were dissolved in the mixture of 96 mL H_2O, 43.1 mL ethanol and 11.2 mL concentrated NH_4OH (28 wt%). Under vigorous stirring, 1.93 mL TEOS was quickly added into the mixed solution at room temperature. After stirring for 1.5 min, this reaction mixture was kept under static condition for 24 h for the complete condensation of silica. After centrifugation at 10,000 rpm and repeated washing by water and ethanol to remove the residual CTAB surfactant, the resulting mesoporous silica nanospheres were obtained and dried at 70 °C.

Next, the MCN was prepared by using the obtained mesoporous silica nanosphere as a hard template in combination with a hydrothermal carbonization method (Titirici et al., 2007). Briefly, 0.75 g mesoporous silica which was previously dehydroxylated by calcination at 800 °C in air was added into 15 mL water containing 0.39 mL furfural. After ultrasonication and stirring for 30 min, the homogenous dispersion was transferred to a 25 mL Teflon-lined stainless steel autoclave and heated to 180 °C for 24 h hydrothermal carbonization reaction. The obtained black product was washed by alcohol and water via repeated centrifugation, and then treated with 4 M HF for removing the silica matrix (*Caution*: *dangerous, handle very carefully!*). After centrifugation and washing by water near to neutral condition, the resulting MCN was obtained and redispersed in water.

Subsequently, 4.0 mg $FeCl_3$, 8.4 mg $K_3Fe(CN)_6$ and 37.2 mg KCl was added into 10 mL 0.05 mg/mL MCN dispersion and stirred for 20 h at room temperature. At this reaction condition, uniform PB nanocrystals could successfully form and block both the surface and nanopores of the MCN nanocarrier to obtain the largest electrochemical response. After centrifugation at 6000 rpm and washing by water for three times, the resulting MCN-PB nanocomposite was obtained and dispersed in 2.0 mL pH 6.0 PBS for further use.

2.4. Preparation of MCN-PB based nanoprobe

Firstly, the MCN-PB dispersion prepared above was added into 2.0 mL 1% PDDA aqueous solution and the mixture was stirred for 30 min to obtain a homogeneous suspension. After centrifugation and washing, the resulting PDDA wrapped MCN-PB nanocomposite was dispersed in 2.0 mL 10 mM PBS. Then, 400 μL of the PDDA wrapped MCN-PB dispersion was added into 3.0 mL colloidal Au NPs prepared by the conventional citrate reduction method (Lai et al., 2009) and mixed gently for 30 min. After washing three times via centrifugation, 20 μg anti-HIgG and 100 μg GOD were added into the resulting MCN-PB/Au NPs nanocomposite which was previously dispersed in 0.80 mL 10 mM pH 6.9 PBS, and gently mixed at room temperature for 2 h followed by storage at 4 °C overnight. Next, the obtained product was centrifuged at 3500 rpm to remove the supernatant and then mixed with 2% BSA for 60 min blocking. After centrifugation and washing with pH 6.9 PBS for three times, the resulting MCN-PB nanoprobe was finally obtained, which was resuspended in 0.8 mL pH 6.9 PBS containing 0.1% BSA and stored at 4 °C.

2.5. Fabrication of immunosensor

Firstly, the SPCE system containing a carbon working electrode (2 mm in diameter), a carbon auxiliary electrode, and an Ag/AgCl reference electrode was fabricated with screen printing technology according to our previous report (Lai et al., 2013). Then, a drop of 40 μL 0.1% $HAuCl_4$ solution containing 0.1 M KCl was applied to the SPCE surface for 100 s electrodeposition at a potential of −0.20 V. After washing by water, 1.0 μL of 0.5 mg/mL anti-HIgG was dropped onto the surface of the working electrode for 12 h assembly in a 100% moisture-saturated environment at 4 °C. Subsequently, the excess antibodies were washed with the washing buffer and a pH 7.0 PBS, and a drop of 20 μL blocking solution was applied to electrode surface for 60 min incubation at room temperature to block possible remaining active sites against nonspecific adsorption. After another washing with washing buffer and PBS, the resulting immunosensor was obtained and stored at 4 °C in a dry environment prior to use.

2.6. Immunoassay procedure

To carry out the immunoreaction and electrochemical measurements, the immunosensor was firstly incubated with a 10-μL drop of the HIgG standard solutions or serum samples for 50 min at room temperature, followed by washing with washing buffer and pH 7.0 PBS. Then, a 10-μL drop of nanoprobe dispersion was cast on the immunosensor surface for another 50 min incubation. After washing with washing buffer and PBS again, 30 μL pH 6.9 PBS containing 10 mM glucose was dropped onto the electrode surface and an electrochemical measurement was performed by differential pulse voltammetry (DPV) from 0.4 to −0.2 V with a step potential of 4 mV, a pulse amplitude of 50 mV, and a pulse period of 0.2 s to record the current response for the quantitative analysis.

3. Results and discussion

3.1. Preparation and characterization of MCN-PB nanocomposite

In order to obtain the MCN nanocarrier, the hard template of mesoporous silica nanosphere with moderately hydrophilic surface was firstly synthesized and filled with the carbon precursor of furfural for applying the hydrothermal carbonization reaction (Gu et al., 2011; Titirici et al., 2007). After removal of the silica template with HF, from SEM images we can find that the obtained MCN well replicated the uniform nanostructure of the mesoporous silica with an average diameter of 180 nm (Fig. 1). Subsequently, this MCN was used as an excellent nanocarrier for the PB loading and nanoprobe preparation. After mixing MCN with $K_3Fe(CN)_6$ and Fe^{3+} and reacting for 20 h, the TEM characterization showed both the nanopores and surface of MCN were fully blocked with a great amount of small nanocrystals (Fig. 1C and D). These nanocrystals should be attributed to the inherent reduction of Fe^{3+} into Fe^{2+} by the MCN (Jin et al., 2010; Cao et al., 2010), which led to the in situ formation of PB nanoparticles on the MCN nanocarrier.

The preparation process of the MCN-PB nanocomposite was also monitored by the FTIR spectroscopy (Fig. 2). Compared with the spectrum of mesoporous silica, two strong absorption peaks at

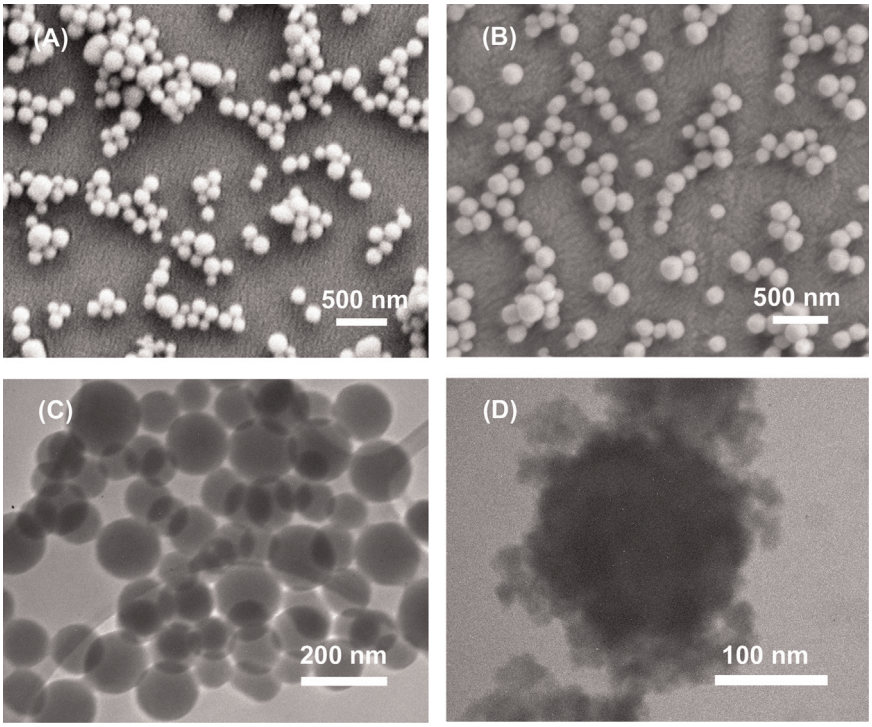

Fig. 1. SEM images of (A) mesoporous silica nanospheres and (B) MCN, and TEM images of (C) MCN and (D) MCN-PB nanocomposite.

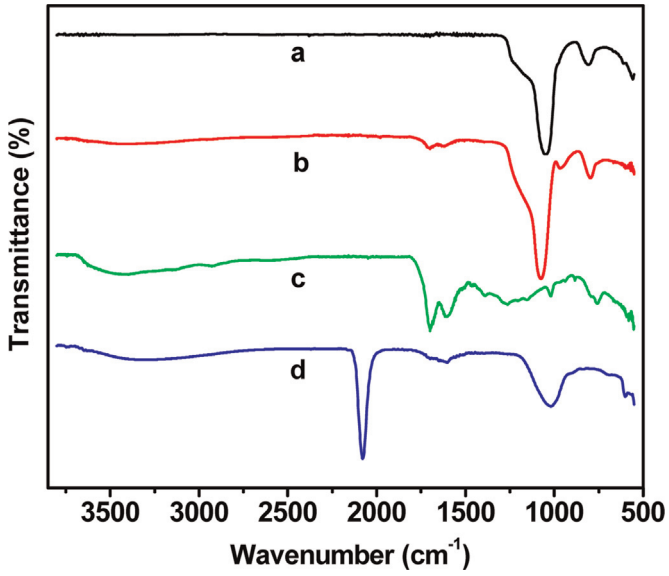

Fig. 2. FTIR spectra of mesoporous silica nanosphere (a), silica-carbon nanosphere (b), MCN (c) and MCN-PB nanocomposite (d).

1697 cm^{-1} and 1605 cm^{-1} as well as a broad absorption band around 3400 cm^{-1} newly appeared as the result of the hydrothermal carbonization reaction on this silica template. These absorption behaviors corresponded to the C=O stretching vibration, C=C stretching, skeletal vibrations as well as the O–H stretching vibration of the produced carbon nanocomposite (Titirici and Antonietti, 2010). After the product was further treated with HF, the Si–O–Si stretching peak at 1050 cm^{-1} completely disappeared whereas the absorption peaks of C=O, C=C vibrations and the broad O–H vibration band well remained. This result demonstrated the successful removal of silica template to form the MCN with abundant oxygen-containing groups (Titirici et al., 2007). After in situ deposition of PB, a strong absorption peak corresponding to the characteristic CN stretching within the complex of Fe^{2+}–CN–Fe^{3+} of PB newly appeared at 2068 cm^{-1} (Jin et al., 2010); meanwhile, the strength of oxygen-containing groups such as the C=O stretching vibration of MCN decreased obviously. These phenomena not only confirmed the successful deposition of PB on the MCN nanocarrier but also suggested that the formation of PB was due to the reduction of the oxygen-containing groups of MCN (Cao et al., 2010; Lai et al., 2014b).

The as-prepared MCN-PB nanocomposite was further characterized with XRD and EDX spectroscopy. The XRD pattern showed obvious diffraction peaks located at $2\theta = 17.21°$, 24.50°, 35.12°, 39.35°, 43.39°, 50.58°, 53.90°, and 57.03° (Fig. S1A), which corresponded to the (200), (220), (400), (420), (422), (440), (600), and (620) reflections of PB, respectively (Jin et al., 2010; Cao et al., 2010). In addition, the EDX spectrum shown in Fig. S1B also demonstrated the presence of related elements of PB such as Fe and K on the obtained MCN-PB nanocomposite. These results further confirmed the in situ formation of PB on the MCN nanocarrier to obtain the MCN-PB nanocomposite successfully.

3.2. Preparation and characterization of MCN-PB based nanoprobe

The abundant oxygen-containing groups of MCN also enabled its good dispersibility in water. As shown in Fig. S2, the as-prepared MCN in aqueous solution (pH 7.0) showed a negative zeta potential of −39.80 mV. After successful deposition of PB on MCN, the zeta potential of the MCN-PB became −53.19 mV (pH 6.0). The negative surface charge allowed the assembly of a layer of positive-charged polyelectrolyte of PDDA on the MCN-PB nanocomposite, which not only provided a tunable surface for the further functionalization but also served as a polymer protection layer to ensure the good stability of PB (Zhao et al., 2005). As a result of PDDA assembly on MCN-PB, its zeta potential reversed to a positive value of +31.85 mV (pH 6.0). Then, this PDDA wrapped MCN-PB nanocomposite could be further assembled by the negative-charged Au NPs synthesized by the conventional citrate reduction method for the nanoprobe preparation (Cui et al., 2008;

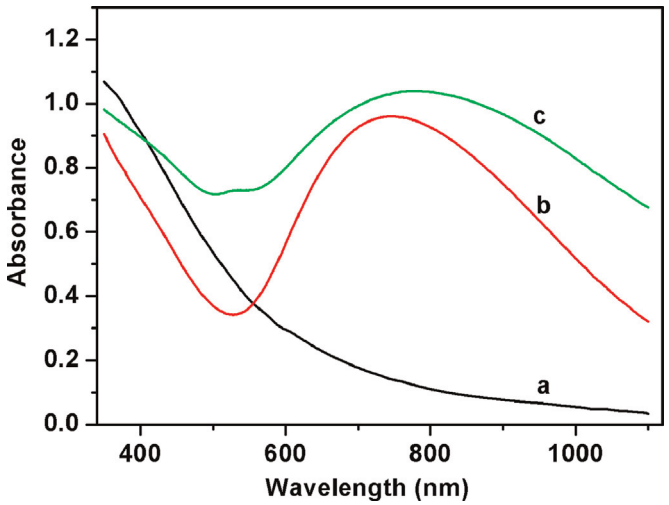

Fig. 3. UV–vis spectra of MCN (a), MCN-PB (b) and MCN-PB/Au NPs nanocomposite (c) dispersed in water.

Lai et al., 2009).

From the UV–vis spectra shown in Fig. 3 we can find an obvious adsorption band around 700 nm which is associated with the charge transfer within the Fe^{2+}–CN–Fe^{3+} of PB (Zhai et al., 2009) on the as-prepared MCN-PB. After the surface coating with PDDA and Au NPs in succession, the resulting product shows a new plasma adsorption peak of Au NPs at 520 nm, indicating the successful preparation of MCN-PB/Au NPs nanocomposite (Cui et al., 2008). Thus, the signal antibody and high-content GOD could be loaded onto this nanocomposite through the inherent interaction between Au NPs and protein biomolecules to obtain the designed nanoprobe (Lai et al., 2009).

The electrochemical behavior of the as-prepared MCN-PB based nanoprobe was investigated by cyclic voltammetry. According to the experiments, the MCN modified SPCE did not show any obvious redox peak in the potential range from 0.4 to −0.3 V (not shown). However, a pair of well-defined redox peaks appeared at the MCN-PB nanoprobe modified electrode in a pH 6.9 PBS (Fig. 4), which should be attributed to the good electrochemical character of PB in situ deposited on the MCN nanocarrier (Zhai et al., 2009; Jin et al., 2010; Cao et al., 2010). Moreover, when 10 mM glucose was added into the PBS solution, this nanoprobe modified electrode showed an obvious electrocatalytic response with great increase of the reduction current. This phenomenon should be ascribed to the sensitive GOD-catalytic response with the electrochemical mediation of PB loaded on the nanoprobe (Lai et al., 2009). This electrocatalytic response could be used for the sensitive signal tracing in the following electrochemical immunoassay.

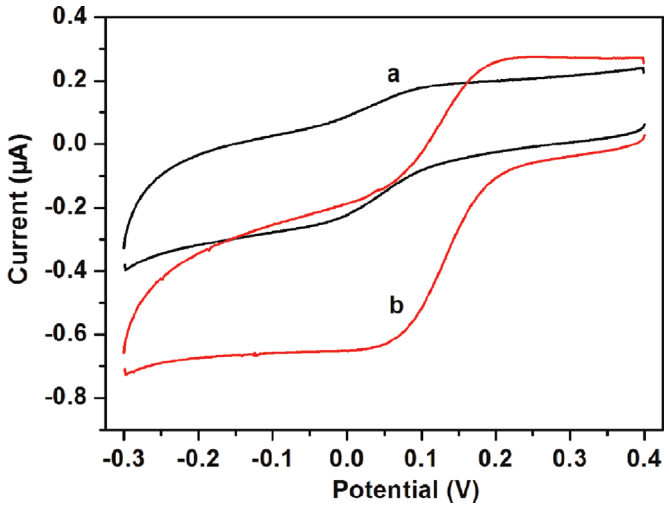

Fig. 4. Cyclic voltammograms of MCN-PB based nanoprobe modified SPCE in a pH 6.9 PBS before (a) and after (b) adding 10 mM glucose. Scan rate: 50 mV/s.

3.3. Electrochemical immunoassay using the nanoprobe

Based on the electrode modification by the electrochemical deposition of Au NPs, anti-HIgG was immobilized on the working electrode surface of a SPCE to form an immunosensor (Zhuo et al., 2008). After a sandwich immunoreaction with the analyte of HIgG and MCN-PB based nanoprobe at the immunosensor in succession, a drop of substrate solution containing excess glucose (10 mM) in a pH 6.9 PBS, at which both the enzymatic bioactivity of GOD and PB stability could be well maintained, was applied to the SPCE surface for the electrochemical measurement. As the GOD on the nanoprobe which was quantitatively captured onto the immunosensing surface through immunoreaction could catalyze the oxidation of glucose substrate with PB as an electron transfer mediator (Lai et al., 2009), sensitive electrochemical signal was produced for the immunoassay (Scheme 1). The high loading of PB and GOD on the nanoprobe as well as the enzymatically catalytic cycle greatly amplified the electrochemical signal, thus this method was able to achieve high sensitivity for the quantitative measurement.

DPV was used to record the sensitive electrochemical response of the immunosensor for quantitative immunoassay. As incubation time is an important factor that affects the analytical performance of an immunoassay method, the DPV current response of the immunosensor toward 100 ng/mL HIgG at different incubation time was investigated. From Fig. S3 we can find that the DPV response of the immunosensor increased with the increasing incubation time used in the sandwich immunoreaction and then reached a constant value after 50 min, which indicated the saturated formation of the immunocomplex. Therefore, an incubation time of 50 min was used for the sandwich immunoassay.

3.4. Analytical performance

The DPV current response of the immunosensor toward the target analyte of HIgG at different concentrations was investigated. As shown in Fig. 5, the DPV response increased with the increase of HIgG concentration, and a good linear relationship between the peak current and the logarithm value of HIgG concentration in the range from 0.01 to 100 ng/mL was obtained with a correlation coefficient of 0.996. The limit of detection at the ratio of signal to noise of 3 was estimated to be 7.8 pg/mL. Based on the comparison listed in Table S1, we can find that this immunosensor has higher sensitivity than many electrochemical immunoassay methods reported previously (Ding et al., 2013; Lai et al., 2014a; Li et al., 2014; Liu et al., 2012; Xu et al., 2012). The excellent analytical performance including wide linear range and high sensitivity of the method is much favorable for its practical applications.

3.5. Specificity, reproducibility, stability and reliability

In order to investigate the specificity of the immunosensor, the electrochemical responses of CEA, MIgG and HSA at the immunosensor were investigated along with the target HIgG (Fig. S4). Compared with the obvious DPV response of HIgG, no obvious current signal over the blank control was observed for CEA, MIgG and HSA samples, which indicated the cross-reactivity of the immunosensor toward noncognate proteins was negligible.

Five immunosensors were prepared and used for the repeated measurements of two different concentrations of HIgG. The

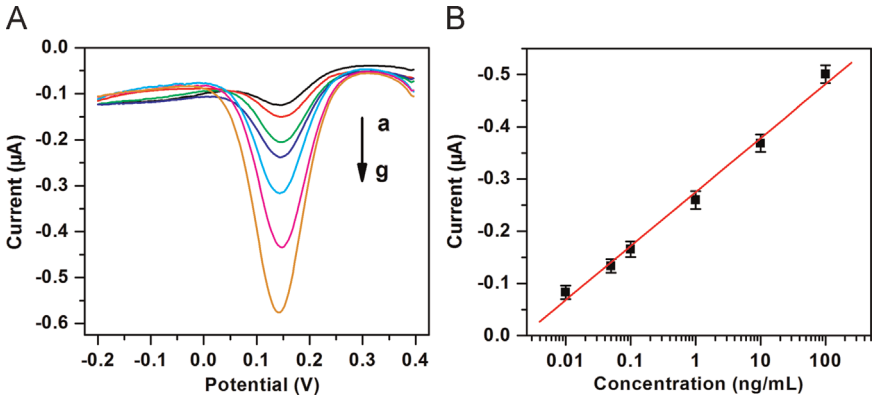

Fig. 5. (A) DPV responses of the immunosensor toward HIgG at different concentrations, and (B) the calibration curve of the method. Curves a–g correspond to the concentrations of HIgG from 0 to 100 ng/mL.

coefficients of variation were 3.5% and 4.3% for the measurements of 0.1 and 10 ng/mL HIgG, respectively. In addition, the immunosensor could retain over 91% of the initial response for 10 ng/mL HIgG after a storage period of two weeks in dry air at 4 °C. When this method was used for the recovery test of HIgG added into the bovine serum sample, acceptable recovery between 97% and 106% was obtained with the relative standard deviation lower than 5.0% (Table S2). These results indicated that the immunosensor had satisfactory reproducibility and stability as well as acceptable reliability for practical applications.

4. Conclusion

A PB–carbon nanocomposite was prepared through the in situ deposition of PB on a newly synthesized MCN nanocarrier less than 200 nm in diameter. The high specific surface area and abundant oxygen-containing groups of MCN arising from the mesoporous silica template and hydrothermal synthesis enabled the in situ deposition of high-content PB and convenient loading of signal antibody and GOD on this nanocarrier to form a useful nanoprobe. Both the high loading of PB and GOD as well as the enzymatically catalytic reaction greatly amplify the signal tracing of electrochemical immunoassay, resulting in the high sensitivity of the method. In addition, the PB-mediated GOD electrochemical system excludes the interference from dissolved oxygen completely. The nanoprobe is low-cost, simple and controllable in preparation. The immunosensor has high specificity and satisfactory reproducibility and stability as well as acceptable reliability. Thus this nanoprobe and the immunoassay method provide great potentials for the practical applications.

Acknowledgments

This work was financially supported by the National Natural Science Foundation of China (21205031 and 21475033), Natural Science Foundation of Hubei Province of China (2014CFB279), State Key Laboratory of Analytical Chemistry for Life Science (SKLACLS1303), and Scientific Research Foundation for the Returned Overseas Chinese Scholars, Ministry of Education of the People's Republic of China (Grant number 2015-49).

Appendix A. Supplementary material

Supplementary data associated with this article can be found in the online version at http://dx.doi.org/10.1016/j.bios.2015.07.026.

References

Cao, L.Y., Liu, Y.L., Zhang, B.H., Lu, L.H., 2010. ACS Appl. Mater. Interfaces 2, 2339–2346.
Chikkaveeraiah, B.V., Bhirde, A.A., Morgan, N.Y., Eden, H.S., Chen, X.Y., 2012. ACS Nano 6, 6546–6561.
Cui, R.J., Liu, C., Shen, J.M., Gao, D., Zhu, J.J., Chen, H.Y., 2008. Adv. Funct. Mater. 18, 2197–2204.
Ding, J.W., Wang, X.W., Qin, W., 2013. ACS Appl. Mater. Interfaces 5, 9488–9493.
Du, D., Wang, L., Shao, Y., Wang, J., Engelhard, M.H., Lin, Y., 2011. Anal. Chem. 83, 746–752.
Fang, Y., Gu, D., Zou, Y., Wu, Z.X., Li, F.Y., Che, R.C., Deng, Y.H., Tu, B., Zhao, D.Y., 2010. Angew. Chem. Int. Ed. 49, 7987–7991.
Gu, J.L., Su, S.S., Li, Y.S., He, Q.J., Shi, J.L., 2011. Chem. Commun. 47, 2101–2103.
Haque, A.M.J., Park, H., Sun, D., Jon, S., Choi, S.Y., Kim, K., 2012. Anal. Chem. 84, 1871–1878.
Hu, B., Wang, K., Wu, L.H., Yu, S.H., Antonietti, M., Titirici, M.M., 2010. Adv. Mater. 22, 813–828.
Ji, L., Guo, Z.K., Yan, T., Ma, H.M., Du, B., Li, Y.Y., Wei, Q., 2015. Biosens. Bioelectron. 68, 752–756.
Jin, E., Lu, X.F., Cui, L.L., Chao, D.M., Wang, C., 2010. Electrochim. Acta 55, 7230–7234.
Karyakin, A.A., Karyakina, E.E., Gorton, L., 2000. Anal. Chem. 72, 1720–1723.
Karyakin, A.A., 2001. Electroanalysis 13, 813–819.
Kim, T.W., Chung, P.W., Slowing, I.I., Tsunoda, M., Yeung, E.S., Lin, V.S., 2008. Nano Lett. 8, 3724–3727.
Lai, G.S., Yan, F., Ju, H.X., 2009. Anal. Chem. 81, 9730–9736.
Lai, G.S., Wu, J., Ju, H.X., Yan, F., 2011. Adv. Funct. Mater. 21, 2938–2943.
Lai, G.S., Zhang, H.L., Yong, J., Yu, A.M., 2013. Biosens. Bioelectron. 47, 178–183.
Lai, G.S., Zhang, H.L., Tamanna, T., Yu, A.M., 2014a. Anal. Chem. 86, 1789–1793.
Lai, G.S., Yin, C.Y., Tan, X.E., Zhang, H.L., Yu, A.M., 2014b. Anal. Methods 6, 2080–2085.
Li, J., Qiu, J.D., Xu, J.J., Chen, H.Y., Xia, X.H., 2007. Adv. Funct. Mater. 17, 1574–1580.
Li, Q.F., Zeng, L.X., Wang, J.C., Tang, D.P., Liu, B.Q., Chen, G.N., Wei, M.D., 2011a. ACS Appl. Mater. Interfaces 3, 1366–1373.
Li, M., Li, W., Liu, S.X., 2011b. Carbohydr. Res. 346, 999–1004.
Li, R., Wu, K.B., Liu, C.X., Huang, Y., Wang, Y.Y., Fang, H.F., Zhang, H.J., Li, C.Y., 2014. Anal. Chem. 86, 5300–5307.
Liu, Y., Liu, Y., Feng, H.B., Wu, Y.M., Joshi, L., Zeng, X.Q., Li, J.H., 2012. Biosens. Bioelectron. 35, 63–68.
Malhotra, R., Patel, V., Vaqué, J.P., Gutkind, J.S., Rusling, J.F., 2010. Anal. Chem. 82, 3118–3123.
Ricci, F., Palleschi, G., 2005. Biosens. Bioelectron. 21, 389–407.
Rusling, J.F., 2013. Anal. Chem. 85, 5304–5310.
Song, S.P., Qin, Y., He, Y., Huang, Q., Fan, C.H., Chen, H.Y., 2010. Chem. Soc. Rev. 39, 4234–4243.
Titirici, M.M., Antonietti, M., 2010. Chem. Soc. Rev. 39, 103–116.
Titirici, M.M., Thomas, A., Antonietti, M., 2007. Adv. Funct. Mater. 17, 1010–1018.
Wan, Y., Min, Y.L., Yu, S.H., 2008. Langmuir 24, 5024–5028.
Wan, Y., Su, Y., Zhu, X.H., Liu, G., Fan, C.H., 2013. Biosens. Bioelectron. 47, 1–11.
Wen, J.L., Zhou, S.G., Yuan, Y., 2014. Biosens. Bioelectron. 52, 44–49.
Xu, Q.N., Yan, F., Lei, J.P., Leng, C., Ju, H.X., 2012. Chem. Eur. J. 18, 4994–4998.
Yang, M.H., Li, H., Javadi, A., Gong, S.Q., 2010. Biomaterials 31, 3281–3286.
Yu, X., Munge, B., Patel, V., Jensen, G., Bhirde, A., Gong, J.D., Kim, S.N., Gillespie, J., Gutkind, J.S., Papadimitrakopoulos, F., Rusling, J.F., 2006. J. Am. Chem. Soc. 128, 11199–11205.
Zhai, J.F., Zhai, Y.M., Wen, D., Dong, S.J., 2009. Electroanalysis 21, 2207–2212.
Zhao, W., Xu, J.J., Shi, C.G., Chen, H.Y., 2005. Langmuir 21, 9630–9634.
Zhuo, Y., Yuan, P.X., Yuan, R., Chai, Y.Q., Hong, C.L., 2008. Biomaterials 29, 1501–1508.